NASA TM X-1375

THEORY AND TESTING OF A SPACE RADIATOR SIMULATOR FOR A SNAP-8 GROUND TEST FACILITY

By Andrew A. Schoenberg, Raymond S. Bilski, and Pierre A. Thollot

Lewis Research Center
Cleveland, Ohio

NATIONAL AERONAUTICS AND SPACE ADMINISTRATION

For sale by the Clearinghouse for Federal Scientific and Technical Information
Springfield, Virginia 22151 – CFSTI price $3.00

THEORY AND TESTING OF A SPACE RADIATOR SIMULATOR FOR A SNAP-8 GROUND TEST FACILITY

by Andrew A. Schoenberg, Raymond S. Bilski, and Pierre A. Thollot

Lewis Research Center

SUMMARY

An analytic and experimental study was made to develop a radiator simulator for the SNAP-8 simulator facility at the NASA Lewis Research Center. The radiator simulation utilized an existing finned-tube heat exchanger cooled by a controllable airflow. The radiator model assumed for the study consisted of a number of parallel finned tubes to which the waste heat of the Rankine cycle was transferred by circulating liquid metal. The same liquid metal, at the flight-temperature levels and flow rates, circulated through the convectively cooled heat exchanger of the simulator facility. The method of simulation was to automatically adjust the coolant air flow of the heat exchanger so that its liquid-metal outlet temperature was at all times the same as that of the radiator model.

Equations for the control of coolant air were derived by linearized analysis of the radiator model and heat-exchanger heat-rejection characteristics. These equations were used in the form of a feedforward (open loop) and feedback controller and were implemented on an analog computer. Feedback integral control on outlet-temperature error was used for accurate steady-state control. Feedforward or open-loop control based on liquid-metal flow and inlet temperature was necessary for controlling the outlet-temperature time response to more rapid disturbances of these two input variables.

Testing the radiator simulator showed that the radiator was accurately simulated for steady-state or very slow transient operation. Transient radiator response to rapid disturbances was also simulated but with less accuracy. The sources of error are traced to the inexact transfer functions and linearizations used to describe the heat-rejection components as well as the simplifications made in the implementation of the control equations. The general requirements for improved transient simulation are discussed.

INTRODUCTION

The development of Rankine cycle space power systems such as SNAP-8 (ref. 1), requires extensive ground testing. In these tests it is not always possible to include all the flight components nor to simulate the space environment. A particular problem is the flight radiator. Flight radiators are usually large and, therefore, have to be operated in a correspondingly large vacuum chamber. Also, the design and construction of vacuum chamber walls, which simulate the heat-sink characteristics of space, are not easy tasks. A simpler approach is to use a radiator simulation in the form of a convectively cooled heat exchanger which is controlled to duplicate the steady-state and dynamic heat-rejection characteristics of the flight radiator. The theory, implementation, and testing of such a radiator simulator used in the SNAP-8 simulator facility at the Lewis Research Center are described in this report.

In the SNAP-8 system, a radiator separate from the condenser is employed to reject the waste heat of the Rankine cycle. This heat is transferred from the condenser to the radiator by circulating NaK (the eutectic of sodium and potassium). In the ground-test facility, the function of the radiator is replaced by two parallel air-blast finned-tube heat exchangers. The coolant airflow to each exchanger is controlled by fast-acting butterfly valves. The problem is to define and implement the controller that will make the heat exchanger operate similar to a specified flight radiator. There is no attempt made to match internal radiator performance. The similarity desired is with respect to the overall heat-transfer rate and specifically to the NaK stream outlet-temperature characteristics in response to NaK flow and inlet-temperature changes. It may be noted that, for the case treated, the design of the ground-test-facility heat exchanger had been determined by considerations other than simulating a particular flight radiator. When the design is not fixed, it is possible to design the heat-rejection system to minimize the control requirements of the radiator simulation. The requirements for such a design are briefly described in the section DISCUSSION OF RESULTS. This report, however, is primarily concerned with defining the controller for a system of fixed design.

The control theory is based on linearized equations - assuming ideal knowledge of both simulated and simulator system. The implementation is, however, simplified because of limited knowledge of the components and the constraints imposed by the control equipment. Such constraints are primarily in the number and types of functions that can be implemented on the analog computer, which is used as the control logic device.

Experimental tests were performed with the aim of evaluating the effectiveness of the radiator simulator. This evaluation includes the ability of the simulator to duplicate the theoretical steady-state input-output characteristics of a typical cylindrical space ra-

diator, as well as the ability to modify the dynamic temperature responses of the finned-tube heat exchangers to match those of the space radiator.

SYMBOLS

C_f total heat capacity of flight radiator (see appendix A)

C_g total heat capacity of ground simulator heat exchangers

C_n specific heat of NaK

E_t error due to inlet temperature change

E_w error due to NaK flow change

e error in NaK outlet temperature of feedback controller, percent of input

F_t normalized transfer function of FHRC relating NaK outlet temperature to inlet temperature

F_w normalized transfer function of FHRC relating NaK outlet temperature to NaK flow changes

f NaK outlet temperature function of FHRC

G_a normalized transfer function of GHRC relating NaK outlet temperature to coolant airflow

G_{ct} transfer function of feedforward controller for changes in NaK inlet temperature

G_{cw} transfer function of feedforward controller for changes in NaK flow

G_f transfer function of feedback loop (see appendix B, eq. (B3))

G_t normalized transfer function of GHRC relating NaK outlet temperature to inlet temperature

G_v transfer function representing air-valve dynamics

G_w normalized transfer function of GHRC relating outlet temperature to NaK flow

g NaK outlet temperature function of GHRC

K proportionality constant used in eq. (16)

K_c gain of integral feedback controller, $\frac{1}{\tau_i}\frac{\partial w_a}{\partial e}\frac{\partial g}{\partial w_a}$

K_{ct} gain of feedforward controller for changes in NaK inlet temperature

K_{cw} gain of feedforward controller for changes in NaK flow

K_f constant in radiator outlet temperature function proportional to sink temperature

K_t ratio of steady-state temperature sensitivities, $\frac{\partial g}{\partial T_i} \Big/ \frac{\partial f}{\partial T_i}$

K_v gain of valve actuator

K_w ratio of steady-state temperature sensitivities, $\frac{\partial g}{\partial w_n} \Big/ \frac{\partial f}{\partial w_n}$

n order of transfer functions

s Laplace transform operator

T_a air coolant inlet temperature, ^oF

T_i NaK inlet temperature, ^oF

T_s space sink temperature, ^oF

$T_n(x)$ local NaK temperature along radiator tube, ^oF

T_{of} NaK outlet temperature of FHRC, ^oF

T_{og} NaK outlet temperature of GHRC, ^oF

t time

w_a coolant airflow, lb/hr

w_n NaK flow, lb/hr

Δw_{af} change in airflow due to feedforward control

x length coordinate of radiator tube

τ time constant (general)

τ_a time constant of G_a function

τ_d time constant of feedback controller command signal filter

τ_i inverse of error integration rate of feedback controller

τ_{tf} time constant of F_t

τ_{tg} time constant of G_t

τ_{wf} time constant of F_w

τ_{wg} time constant of G_w

τ_1, τ_2 time constants of feedback loop dynamics (see appendix B)

ω frequency, rad/sec

Conversion factors from U.S. Customary to metric units:

Multiply	By	To obtain
pounds	0.4536	kilograms
feet	0.3048	meters
Btu	1054.8	joules
pounds per second	0.4536	kilograms per second
Btu per ^{o}F	1900	joules per ^{o}C
Btu per pound per ^{o}F	4190	joules per kilogram per ^{o}C
$^{o}F-32$	5/9	^{o}C

DIFFERENCES BETWEEN FLIGHT RADIATOR AND AIR-COOLED HEAT EXCHANGER

The first step in defining the requirements of a radiator simulator is to examine the differences between a flight radiator for SNAP-8 and the test facility heat exchanger. The construction of the two heat-rejection components is described and their thermal characteristics are compared.

The flight radiator assumed for this study (hereinafter referred to as FHRC, flight heat-rejection component) is shown schematically in figure 1. It consists of 130 parallel tubes each with two solid longitudinal fins; the NaK flow is assumed to be equally distributed among the tubes. The heat is conducted from the NaK through the tube walls, armor, and fins, and then radiated to space. The particular configuration presented in not necessarily the final flight version in that both the mission and the booster chosen will affect the final design. For the purpose of analysis, the cylindrical radiator shown is representative in terms of fin area and weight.

The test facility heat-exchanger system or ground heat-rejection component (referred to hereinafter as GHRC) shown in figure 2 consists of two parallel heat exchangers each containing 28 parallel finned tubes. The heat from the NaK flowing inside the tubes is conducted to the fins, which are convectively cooled by air. To ensure uniform cooling, a perforated baffle plate is located in the inlet air ducting of each element of the GHRC. The airflow to each exchanger can be adjusted by electropneumatically operated butterfly valves.

The effects due to differences in construction and mode of heat transfer are manifested in different steady-state and transient NaK temperature characteristics for each system. The steady-state differences in the input-output NaK temperature characteristics for two levels of NaK flow are shown in figure 3. The solid lines represent the

theoretical characteristic for the FHRC at constant NaK flow in the sun. The data points and the dashed lines drawn through them represent the experimentally determined temperature characteristic of the GHRC at a constant airflow. The divergence of the dashed and solid lines indicates that the sensitivity of the NaK outlet temperature to changes of inlet temperature is greater for the GHRC than for the FHRC. Transient characteristics for the two heat-rejection components also differ, as suggested by the differences in their heat capacities and NaK dwell times shown in table I. Calculations of the heat capacities are shown in appendix A. Comparison of the values shows that the total heat capacity and dwell time are about four times larger for the FHRC than for the GHRC. The NaK outlet temperature transient response of the FHRC should be correspondingly slower, as can be seen in figure 4. The dashed curve in the figure is the measured NaK outlet temperature response of the GHRC to a step change in NaK flow: The solid curve is the corresponding response of an analog computer simulation of the FHRC. The method of simulation is discussed in the next section. Note that it takes approximately four times longer for the radiator to reach 50 percent of the steady-state value.

The foregoing examination has indicated that to make the response of the heat-rejection components similar requires a control system that will modify considerably both the steady-state and dynamic characteristics of the GHRC. The form of such a controller is considered next.

RADIATOR SIMULATOR CONTROL SYSTEM

Control Concept

Because the SNAP-8 simulator facility heat-rejection loop was operated at flight-system flows, temperature, and power levels, the problem of simulating the radiator was reduced to controlling the GHRC coolant air so that the temperature of the NaK emerging from the heat exchangers was at all times the same as it would be for the flight radiator. More precisely, for every change in NaK flow w_n or inlet temperature T_i, the controller must change the airflow w_a so that the variation of the GHRC outlet temperature function $g(T_i, w_n, T_a, w_a, t)$, is equal to the variation of the radiator outlet-temperature function $f(T_i, w_n, T_s, t)$. The air temperature T_a, included in the g function for generality, represents a disturbance variable acting on the GHRC. Also for generality, the function f contains the sink temperature T_s, although its variations were not treated in this study.

The control-system concept in block-diagram form is shown in figure 5. The command signal to the airflow valves is provided by both a feedback controller, which controls according to the NaK outlet temperature error, and a feedforward or open-loop

controller, which controls according to the variations in NaK flow and inlet temperature. The feedback loop acts as an accurate steady-state temperature control compensating for distrubances not provided for in the feedforward control (such as variations in T_a) and for simplifications made in the component modeling. Unfortunately, the feedback controller is slow acting for loop gains consistent with stability, so that only slow disturbances can be controlled with this mode alone. The frequency range over which it is effective is discussed in the Feedback Integral Controller Test section. The feedforward control is necessary for effective control of the GHRC transients. This mode of control is faster because it responds to input disturbances without waiting to sense an error in outlet temperature. The form of this feedforward controller is derived in the next section.

Equations of Feedforward Controller

The change in airflow due to the feedforward controller can be expressed in linearized form by equation (1)

$$\Delta w_{af} = K_v G_v (K_{cw} G_{cw} \Delta w_n + K_{ct} G_{ct} \Delta T_i) \tag{1}$$

where the K's represent gains of the various control elements and the G's represent normalized transfer functions or the time-dependent relation of each element. As an example, $K_v G_v$ represents the air-valve and actuator characteristics. The feedforward controller is made up of two elements represented by $K_{cw} G_{cw}$ and $K_{ct} G_{ct}$. The first element responds to NaK flow changes; the second element responds to NaK inlet temperature changes. The structure of these controller elements is fixed by the requirement that the transient error between the outlet temperature of the GHRC and FHRC be zero. In linearized form, the error is given by

$$\Delta T_{of} - \Delta T_{og} = \left(\frac{\partial f}{\partial w_n} F_w - \frac{\partial g}{\partial w_n} G_w \right) \Delta w_n - \frac{\partial g}{\partial w_a} G_a \Delta w_a + \left(\frac{\partial f}{\partial T_i} F_t - \frac{\partial g}{\partial T_i} G_t \right) \Delta T_i \tag{2}$$

Note that only variations in NaK flow, inlet temperature, and airflow are considered. The other variables T_s and T_a are assumed to be constant. The partial derivatives represent the steady-state sensitivities of the ground and flight systems and the G's and F's are the corresponding normalized transfer functions. If the airflow is varied according to the feedforward relation given by equation (1), the temperature error can be rewritten as follows:

$$\Delta T_{of} - \Delta T_{og} = \left(\frac{\partial f}{\partial w_n} F_w - \frac{\partial g}{\partial w_n} G_w - \frac{\partial g}{\partial w_a} G_a K_v G_v K_{cw} G_{cw} \right) \Delta w_n$$

$$+ \left(\frac{\partial f}{\partial T_i} F_t - \frac{\partial g}{\partial T_i} G_t - \frac{\partial g}{\partial w_a} G_a K_v G_v K_{ct} G_{ct} \right) \Delta T_i \qquad (3)$$

To obtain the zero temperature error for all changes of NaK flow and NaK inlet temperature, the coefficients of Δw_n and ΔT_i in equation (3) must be zero. This requirement results in two equations for the two unknown elements of the feedforward controller:

$$K_{cw} G_{cw} = \left(\frac{\partial f}{\partial w_n} F_w - \frac{\partial g}{\partial w_n} G_w \right) \frac{1}{\frac{\partial g}{\partial w_a} G_a K_v G_v} \qquad (4)$$

$$K_{ct} G_{ct} = \left(\frac{\partial f}{\partial T_i} F_t - \frac{\partial g}{\partial T_i} G_t \right) \frac{1}{\frac{\partial g}{\partial w_a} G_a K_v G_v} \qquad (5)$$

The required control action can be seen from the form of the equations. The terms within the parentheses represent differences in the response of the two heat-rejection components to each of the two input variables. If any of the sensitivities and dynamic characteristics were the same for the GHRC and the FHRC (e.g., if $(\partial f/\partial w_n) = (\partial g/\partial w_n)$ and $F_w = G_w$), G_{cw} would be zero and, as expected, no control for NaK flow changes would be required. This, however, is not the case. Hence, the feedforward controller takes on a nontrivial form. The term outside the parentheses, which is the same for both equations, represents the compensation required to overcome the dynamics of both the valve G_v and the NaK outlet-temperature to the airflow-transfer function G_a. Note that, although there are two valves and two heat exchangers in the actual system, one transfer function suffices to describe their parallel operation.

At this stage, the form of the feedforward controller is still general to the extent that the G's and F's as well as the partial derivatives and gains could describe any radiator and heat-exchange system; also, the term $[(\partial g/\partial w_a) G_a K_v G_v]$ could represent any dynamics interposed between the controlled variable and the manipulated variable. To define the specific controller for this particular radiator simulator, however, the transfer functions of both the GHRC and FHRC must be determined.

Transfer Functions for Feedforward Controller

The five transfer functions that relate the NaK outlet temperature of the heat-rejection components to the NaK flow, inlet temperature, and airflow were determined by assuming each to be of the general form $\left[1 + (\tau s/n)\right]^{-n}$, where s is the Laplace operator, τ is the time constant, and n is the order of the transfer function. The simple two-parameter structure is admittedly an approximation to the complex dynamics of the heat-rejection components. Nevertheless, it was assumed that specification of the time constants and the orders of the responses was sufficient to define the essential structure of the feedforward controller. The particular transfer functions, as used in the controller equations, are given as follows:

$$G_a = \left(1 + \frac{\tau_a s}{2}\right)^{-2} \tag{6}$$

$$G_w = \left(1 + \tau_{wg} s\right)^{-1} \tag{7}$$

$$G_t = \left(1 + \frac{\tau_{tg} s}{3}\right)^{-3} \tag{8}$$

$$F_t = \left(1 + \frac{\tau_{tf} s}{3}\right)^{-3} \tag{9}$$

$$F_w = \left(1 + \frac{\tau_{wf} s}{2}\right)^{-2} \tag{10}$$

Table II lists the values of the time constants used for the simulator tests and the method of determining each. The pertinent system parameters used for the calculations correspond to the typical steady-state values in the operating range of the tests.

The time constants τ_a and τ_{wg} for the GHRC transfer functions G_a and G_w, respectively, were determined from experimental responses to step changes in airflow and NaK flow. These responses are shown in figures 6 and 7, respectively. Note that the two responses corresponding to each of the heat exchangers of the GHRC are shown. The changes of opposite polarity were purposely made so that the combined NaK outlet stream temperature remained unchanged. As a result, no significant changes occurred in the GHRC NaK inlet temperature, which would otherwise have confounded the re-

sponse to inlet temperature with the response to airflow or NaK flow. Note, also, that the close similarity between the positive and negative step responses indicates that, for this variation, the system does not deviate significantly from linearity. The time constants τ_a and τ_{wg} were chosen so that the integral errors between the experimental responses and the transfer-function approximations were zero. This criterion was simple to implement since τ is then equal to the shaded area between a hypothetical, instantaneous response and the experimental response when normalized by the total change in temperature. This equality between τ and the control area (ref. 2) is independent of the choice of n, as shown for a general transfer function in reference 2. The step responses of the assumed transfer functions are shown by the solid lines in the figures. The n's of the transfer functions were chosen for the best fit in shape to the experimental responses. The slight difference in control area apparent in figure 7 is a result of the fact that the experimental control area was not measured accurately at the time it was first used to formulate the G_w function.

The time constants of the remaining three transfer functions were estimated by use of the formulas shown in the table II. These formulas were developed by analysis of the relation between the control area of the NaK outlet-temperature response and the change of internal energy of the heat-rejection component undergoing the transient. The analysis indicated that the primary variables determining the control area were the effective heat capacity of the heat-rejection component and the NaK flow rate. These formulas are not exact; however, posttest analysis and studies with a digital computer simulation of the flight radiator substantiated that the form of the formulas was essentially correct and that values of time constants calculated thereby were in fairly good agreement with those measured from the step responses of the computer simulation. The degree of agreement in control area and shape can be seen in figure 8 which shows the step response of the computer simulation and the response generated by the transfer-function approximation for F_t and F_w. In the figure, F_t does not agree well in shape because of the low-order approximation used. A higher order was not implemented in order to conserve analog computer capacity. The error involved is not considered serious because the low-frequency behavior, which is of primary interest, is represented by the low-order approximation. The same third-order form was used for G_t. The time constant τ_{tg} was calculated by using the formula given in table II. Note that in this formula the first term can also represent the theoretical expression for τ_{wg}. Instead of using the calculated value, however, the experimentally determined value of τ_{wg} was used for determining τ_{wf}. It was felt that this gave a more accurate value for the time constant since the theoretical formula gave a value for τ_{wg} which was about 10 seconds less than the measured value.

The transfer function representing the dynamics of the airflow valve and actuator, G_v, was approximated by 1. This approximation was justified because valve tests indi-

cated that only 3 seconds were required for the valve to go from the fully opened to the fully closed position, so that its dynamics were insignificant in comparison with G_a.

Implementation of Control System

Feedforward controller. - The five transfer functions given by equations (6) to (10) were substituted into equations (4) and (5) to determine the final structure of the feedforward controllers. The result, with the numerical values of the time constants inserted, is expressed in the following equations:

$$K_{cw}G_{cw} = \left[\frac{\partial f/\partial w_n}{K_v(\partial g/\partial w_a)}\right]\left[\frac{(1 + 33.5\ s)^2}{(1 + 60\ s)^2} - \frac{K_w(1 + 33.5\ s)^2}{(1 + 48\ s)}\right] \tag{11}$$

where

$$K_w = \frac{\partial g/\partial w_n}{\partial f/\partial w_n}$$

$$K_{ct}G_{ct} = \left[\frac{\partial f/\partial T_i}{K_v(\partial g/\partial w_a)}\right]\left[\frac{(1 + 33.5\ s)^2}{(1 + 63.3\ s)^3} - \frac{K_t(1 + 33.5\ s)^2}{(1 + 25\ s)^3}\right] \tag{12}$$

where

$$K_t = \frac{\partial g/\partial T_i}{\partial f/\partial T_i}$$

Note that G_a has been brought inside the brackets so that a lead-lag form results. In this simplified form, only the second term inside the brackets of equation (11) (where the lead term is second order and the lag is first order) poses a problem in regard to implementation. This term theoretically requires differentiation of the input signal, which is not practical when the noisy flow signals generated by the experimental facility are considered. Hence, a compromise first-order approximation was used for the second-order lead term. The resulting feedforward controller for NaK flow is given by

$$K_{cw}G_{cw} = \left[\frac{\partial f/\partial w_n}{K_v(\partial g/\partial w_a)}\right]\left[\frac{(1 + 33.5\ s)^2}{(1 + 60\ s)^2} - K_w\frac{(1 + 67\ s)}{(1 + 48\ s)}\right] \tag{13}$$

An additional simplification was made on the NaK inlet-temperature control element (eq. (12)); the lead and lag elements of the second term were canceled. This cancellation was assumed to be justified because the control area of the lead term was nearly equal to that of the lag term. The resultant simplified form of the NaK inlet temperature control element is given as

$$K_{ct}G_{ct} = \left[\frac{\partial f/\partial T_i}{K_v(\partial g/\partial w_a)}\right]\left[\frac{(1 + 33.5\ s)^2}{(1 + 63.3\ s)^3} - K_t\right] \tag{14}$$

Equations (13) and (14) represent the feedforward controller that was programed on the analog computer.

Feedback controller. - The feedback controller used in the simulation employed a simple integrator with variable integration rate as the controller. The command signal representing the desired NaK outlet temperature of the flight radiator was generated by a formulation of a steady-state radiator equation on the analog computer. The required relation of outlet temperature to both the inlet temperature and flow, is given by equation (15).

$$1 - \frac{T_{of}^3}{T_i^3} - \frac{K_f}{w_n}T_{of}^3 = 0 \tag{15}$$

(Note that the absolute temperature scale must be used.) This relation is obtained from equation (16) which approximates the steady-state temperature gradient of NaK flowing through a tube while losing heat by radiation:

$$\frac{dT_n(x)}{dx} = -\frac{K}{w_n}T_n^4(x) \tag{16}$$

Integration of this equation between the limits T_i to T_{of} results in equation (15). The constant K_f depends on the space sink temperature and the length of the radiator tube. This constant was adjusted to match the radiator characteristics shown in figure 3. The transient characteristics of the radiator did not need to be simulated since the feedback element was intended to act only as a steady-state control. Nevertheless, a large lag

(with a time constant τ_d of 100 sec) had to be added to the output of the temperature command signal to prevent sending premature signals to the feedback control in response to NaK inlet temperature and flow changes. The value of 100 seconds was chosen because it was in the range of the flight radiator time constants. At the same time, the resultant lag was not slow enough to prevent effective feedback control action.

The complete control system is shown as a block diagram in figure 9. Figure 10 presents the corresponding circuits programed on the analog computer. Note that first-order lag filters (time constant = 1 sec) are added to the input signals shown in figure 10. These filters eliminate much of the high-frequency noise present in the measured signal. The potentiometer settings of the analog computer were fixed by values of the time constants and coefficients as specified by the analysis. Potentiometer settings and the formulas used to determine them are presented in table III. Although the gains of the feedforward circuits (potentiometers 14 and 16) could also be calculated from theory, it was simpler to determine their proper setting by experimentation. The effect that these two gains and the feedback controller gain (potentiometer 68) have on the simulator transients is considered in the next section.

RADIATOR SIMULATOR TESTING

The tests were performed in the SNAP-8 simulator facility which included three complete liquid-metal loops rated for flight power level operation. A brief description of this system is presented to aid in understanding the radiator simulator tests. The schematic diagram of the system showing the type and location of the more important instrumentation is shown in figure 11. The first loop transfers the heat from a reactor simulator to the boiler. This heat vaporizes the mercury circulating in the second loop, which represents the actual Rankine cycle. After passing through the turbine simulator, the mercury condenses in the compact condenser cooled by the third loop, NaK. The NaK transfers the waste heat to the radiator simulator where it is finally rejected to the atmosphere by the cooling air.

The instrumentation included Chromel-Alumel thermocouples, both Bourdon tube and strain-gage pressure measuring devices, and electromagnetic flowmeters for measuring all the variables of interest in the heat-rejection loop. Most of the thermocouples were attached on the outside of the tube walls, which introduced a few seconds of lag in the measurement of the NaK temperature transients; however, this error was not serious because such transients generally involved time constants of 30 seconds to 10 minutes. Both total NaK flow and the NaK flow through one of the heat exchangers of the GHRC were measured by electromagnetic flowmeters, which may be assumed to have insignificant lag. The airflow in the heat exchangers was measured indirectly by the pressure

drop through a calibrated orifice. The accuracy of the airflow and air-temperature measurements did not enter into the radiator simulator evaluation, only the polarity and shape of the time response of the coolant flow was of interest.

The variables were recorded by various methods. A six-channel pen recorder was used for continuous recording of the NaK inlet and outlet temperatures, the total NaK flow rate, and three of the analog computer controller signals. Panel meter readouts of various system temperatures, pressures, and flows provided convenient monitoring of overall loop operation. Steady-state system data were recorded by a 350-channel, centralized, digital data system (ref. 3). A higher speed (18.75 data points/sec), 20-channel, modified version of this system was used for recording transient data.

The tests were performed to evaluate the steady-state and dynamic characteristics of the feedforward and feedback controllers and to determine the circuit gains that produce the best simulation of the space radiator. The transient responses of the radiator simulator were later compared with the expected radiator response to evaluate the effectiveness of the simulation. Two types of transient tests were performed. Step changes in mercury flow were used to introduce NaK inlet temperature disturbances to the radiator simulator; however, because of the condenser and the system-piping heat capacity, the resultant NaK temperature changes were rather slow. In contrast, fast changes approaching a step in NaK flow could be achieved to test the radiator simulator response to this variable.

Feedback Integral Controller Test

The feedback integral controller in conjunction with the radiator command signal generator was tested to evaluate (1) how well it generated the desired steady-state characteristics and (2) to what extent it influenced the dynamic response of the radiator simulator.

Steady-state characteristics of the GHRC with the integral controller operating are shown in figure 12 (feedforward controllers disconnected). The data points represent the experimental performance of the radiator simulator under steady-state conditions. The solid lines are the desired radiator characteristics previously shown in figure 3. The excellent agreement demonstrates that known steady-state flight radiator characteristics can be simulated. It follows that, for all transient tests, the initial and final values of the GHRC outlet temperature will be correct when the integral controller is operating.

The dynamic performance of the feedback controller was evaluated by introducing inlet-temperature transients and recording the GHRC outlet temperature response for various integrator gain settings (potentiometer 68). These transients were generated by

making a step change in the mercury flow which resulted in the subsequent change of the GHRC NaK inlet temperature. Figure 13 shows this NaK inlet temperature forcing function and the resulting NaK outlet temperature response for three feedback controller conditions. (The feedforward controller was disconnected for these tests.) The uppermost response curve, for which the integration rate was set to zero and no feedback control action was present, attains a steady-state value of outlet temperature which corresponds to the uncontrolled heat-exchanger characteristic shown in figure 3. When feedback integral control is applied, as shown by the remaining two curves, the desired steady-state radiator outlet temperature, corresponding to the characteristic of figure 12, is attained. In general, the tests show that, as the integration time decreases (to about 50 sec), the steady state is attained more rapidly; however, for smaller integration times, the response becomes oscillatory. Thus, satisfactory control on only slow disturbances is possible with the feedback control. The speed of these disturbances can be estimated by frequency response analysis. The calculations are given in appendix B. The resulting frequency response with integral control adjusted for critical damping is shown in figure 14. The plot shows the error in the NaK outlet temperature (in percent of the amplitude of the input signal) as a function of frequency. For generality, the frequency is normalized by the period equal to $1/2\ \tau_a$ of the transfer function G_a. It may be seen from the figure that the error is small only for low-frequency disturbances. For example, the error is reduced to 50 percent for $\omega\tau_a/2$ equal to 0.08. If τ_a is equal to 67 seconds, this requires the input disturbance frequency to be 0.0024 radian per second before the error is reduced to half the no-control value. Hence, only extremely slow distrubances can be controlled by the feedback controller. The control of more dynamic disturbances must be left to the feedforward controller.

Test of Feedforward Controller with Changes in NaK Inlet Temperature

Each of the feedforward controller elements was tested separately. The element that senses NaK inlet temperature changes was tested by stepping the mercury liquid-flow. The results of a typical test, as recorded on the pen recorder, are presented in figure 15. The curve in part (a) is the NaK inlet temperature which represents the forcing function acting on the radiator simulator. The curve in part (d) is the corresponding NaK outlet temperature response. The two additional traces (figs. 15(b) and (c)) represent the control signals to the radiator simulator. The principal effect of the feedforward signal (fig. 15(b)) is to slow the initial outlet-temperature response of the GHRC heat exchangers. This maneuver is achieved by a rapid increase in the control signal which peaks immediately after the start of the transient and then diminishes to zero as the rate of inlet-temperature change decreases. The feedback integral control in the

meantime has integrated the temperature error and begins generating the signal, which eventually drives the GHRC outlet temperature to the equivalent FHRC outlet temperature. Note that according to equation (14), the feedforward circuit should generate a steady-state signal proportional to the value of $1 - K_t$. However, the value of K_t was adjusted to 1 so that the steady-state value of NaK outlet temperature was only a function of the feedback control. The error in the dynamic response introduced by this simplification is not serious in that the estimated value of K_t is approximately 1.3, and the feedback controller compensates the required steady-state signal. The nonoscillatory response of both the total control signal and the outlet temperature in figure 15(c) indicates that the combined control system was functioning properly.

The amount that the initial transient is slowed varies with the gain of the feedforward controller. To determine the best gain setting, a number of values were tried. The resultant variations in NaK outlet temperature response for identical inlet perturbations are shown in figure 16. As expected, the control area increases with the gain. The output response that is desired, as generated by the transfer function F_t (eq. (9)), is shown as the dashed line in the figure. Although none of the simulator responses accurately follow the desired response, the shape and trend of the data indicate that, with the proper gain, the desired response can be attained. Note that the desired response is an approximation of the real radiator response generated by the transfer function F_t used in the synthesis of the controller. Comparison with the inexact transient is appropriate because it evaluates the controller according to its theoretical capability.

Test of Feedforward Controller for Changes in NaK Flow

The performance of the feedforward circuit operating on NaK flow was tested by introducing step changes in that variable. Although these disturbances are more severe than those normally encountered in system operation, step changes facilitated the evaluation of controller dynamics. To prevent simultaneous changes in NaK inlet temperature, which result when the total loop flow is changed, flow distrubances of opposite polarity were introduced to the individual GHRC heat exchangers, as discussed in the previous section on determination of the time constants. A typical transient is shown in figure 17. The traces in figure 17(d) show the positive and negative step changes in the NaK flow rate in heat exchangers 1 and 2, respectively. The corresponding transients in airflow rate (fig. 17(b)) are caused by the feedforward controller in response to the NaK flow changes. The airflow transients slow down the NaK outlet-temperature response. These temperature traces are shown in figure 17(a). The effect of the airflow can be seen in the temperature responses in the region between 50 and 120 seconds where the change in temperature is completely arrested by the action of the coolant. Note that the

NaK inlet temperature which is common to both heat exchangers remains constant as desired. The data points shown are samples taken by the digital recording system. The actual sampling rate and the scatter are indicated by the high density of data points in the interval between 80 and 90 seconds of the recording. The integral-feedback controller was disconnected for these tests, because it was inoperable when the individual heat exchangers were acting against each other to prevent changes in NaK outlet temperature. Also, as in the previous transient tests, the feedforward controller was active only during the transient. This was achieved by adjusting K_w in equation (13) to 1.

The NaK outlet-temperature response for various values of gain (potentiometer 14 of the analog circuit) is shown in figure 18. The dashed line represents the desired response generated by the analog computer model of F_w. Although the desired control area can be obtained by adjusting the gain, the shapes of the responses indicate that the control action is insufficient during the first 10 to 20 seconds of the transient. This may be attributed to the fact that the NaK outlet-temperature responds more slowly to airflow changes than to NaK flow changes. Analytically, this difference was indicated by the higher order of G_a relative to G_w. To overcome this extra lag, it may be recalled that the second term in brackets of equation (11) required differentiation of the input flow signal. Such differentiation was, however, not practical because of the noisy input signals generated by the experimental facility. The compromise first-order lag, which was actually implemented, is apparently not fast enough for step changes in NaK flow. Improvement in the shape of the response could be obtained by a better approximation to the required differentiation. The efficacy of such modifications in the controller structure, however, would have to be demonstrated experimentally.

DISCUSSION OF RESULTS

The test results have shown that the specified radiator, NaK outlet-temperature characteristics can be simulated accurately under steady-state conditions and for slow variations in the input variables. This control action can effectively be performed by an integral feedback controller. Its limitation lies in the control of fast disturbances, where feedforward control must be relied on.

This feedforward control was tested with various transients, and it demonstrated the ability to slow the NaK outlet-temperature response to near the desired values. Because of particular limitations of the system tested, however, the full potential of this technique could not be realized. For one thing, the dynamics of the heat-rejection components were not known accurately nor could they be implemented in the exact form required by the feedforward controller theory. These limitations affected both feedforward circuits. In one case, it was necessary to approximate the NaK outlet- to inlet-

temperature response with a third-order transfer function. In the second case, the required differentiation of the flow signal could not be implemented. These problems, however, are not insurmountable and may, for many systems, not exist at all. Usually, more accurate representation of the heat-rejection components with a reasonable increase in analog computer equipment may be obtained. The troublesome differentiation is not required at all for heat exchangers where the outlet temperature responds to the manipulated variable as fast as or faster than to the disturbance variables. When differentiation is required, better approximations of this operation may be implemented with proper filtering, particularly if the inputs are slower than step changes. In this connection, it may be noted that the low-order transfer-function approximations used for the controller are more representative of the system dynamics for slow (low frequency) disturbances. Hence, it may be expected that the simulator will, in general, perform better for the less severe transients encountered during realistic power-system operation.

The testing was carried out essentially around one operating point for which the assumptions used in the synthesis of the controller were approximately valid. The question remains of how the radiator simulator performs under wide variations of operating point, such as encountered during startup of the system. The feedback controller and, hence, the steady-state operation would not be affected since the integration error does not depend on the assumption of linearity, and the command signal is generated by the nonlinear equations. The feedforward circuit parameters are, however, particularly dependent on the value of NaK flow level. This means that the gains and some of the time constants of the controller circuit may have to be varied according to flow rate. To what extent and how this would be done remains to be studied.

It should be pointed out that the method of radiator simulation presented herein was developed with the assumption that the design of the GHRC was given and fixed. This meant that the controller served to change the operating characteristics of the given heat exchangers to conform to the desired operating characteristics of a flight radiator. When the component design is not fixed and when the required flight characteristics can be predicted and specified, it is possible to construct the heat exchanger of the GHRC so that the control requirement is minimized. The control requirement, expressed in linearized form by equations (4) and (5), is minimized when the simulator heat exchanger is designed so that its transfer function representation becomes the same as that of the radiator. In this connection, one parameter that is essential for dynamic similarity is the heat capacity. It enters directly into the equations for determing the time constant or control area of the transfer-function representation. Unless the heat capacity, which determines the energy storage capability of the heat exchanger, is approximately equal in both systems, dynamic similarity can be achieved only by an active and sometimes complex control system. Other factors, such as the heat-transfer coefficients and fin geom-

etry also influence the dynamic response and need to be considered; however, their effect on the dynamic response is of secondary importance.

CONCLUSIONS

Evaluation of the radiator simulator for the SNAP-8 simulator facility at the Lewis Research Center has led to several conclusions. The steady-state characteristics of a typical flight radiator can be simulated satisfactorily with a convectively cooled heat-exchanger by using an integral feedback control in conjunction with a single temperature command signal representing the desired radiator outlet temperature. The feedback control is, however, ineffective in controlling the transient characteristics.

A feedforward or open-loop control must be used where the dynamic characteristics of the ground-system heat exchanger differ significantly from those of the flight radiator, as in the case studied in this report. This feedforward control was implemented to simulate the radiator transients in NaK outlet temperature caused by NaK flow and inlet temperature changes. It was effective in slowing the response of the ground heat-rejection system to approximate the predicted response of the flight radiator. The accuracy of this approximation was, however, limited by several factors. These include (1) the difficulty in accurately characterizing the dynamics of both the flight radiator and the ground heat exchangers, and (2) the limitations in capacity and complexity of the control equipment that was available for the tests. Evaluation of these limitations indicates that none of them are insurmountable but that more equipment and testing would be needed for more accurate simulation of the radiator.

Analysis of the controller equations led to the further conclusion that the open-loop control may be greatly simplified for systems where the simulator heat exchanger can be designed according to the known radiator characteristics. One important design criterion for similarity in response is making the heat capacity of the ground heat-rejection component the same as that of the radiator. Further study is needed to establish more exact design criteria.

Lewis Research Center,
National Aeronautics and Space Administration,
Cleveland, Ohio, January 23, 1967,
701-04-00-02-22.

APPENDIX A

CALCULATIONS OF HEAT CAPACITIES OF FLIGHT AND GROUND HEAT-REJECTION COMPONENTS

130-Tube Flight-Radiator Heat Capacity

Tubes and Armor:

$$M_{tf}C_{tf}n_{tf} = (6.44)(0.333)(130) = 278 \text{ Btu/}^{o}\text{F}$$

where M_{tf} is the mass of the tube in the flight radiator, C_{tf} is the specific heat of the tube of the flight radiator, and n_{tf} is the number of tubes in the flight radiator.

Fins:

$$M_{ff}C_{ff}n_{ff} = (1.49)(0.215)(260) = 83.2 \text{ Btu/}^{o}\text{F}$$

where M_{ff} is the mass of the fin of the flight radiator, C_{ff} is the specific heat of the fin of the flight radiator, and n_{ff} is the number of fins in the flight radiator.

NaK Inventory:

$$M_{nf}C_{n} = (53.8)(0.21) = 11.3 \text{ Btu/}^{o}\text{F}$$

where M_{nf} is the mass of NaK in the flight radiator and C_{n} is the specific heat of NaK.

56-Tube Simulator Heat-Exchanger Heat Capacity

Tubes:

$$V_{wg}\rho_{wg}C_{wg}n_{tg} = (0.0094)(500)(0.11)(56) = 28.9 \text{ Btu/}^{o}\text{F}$$

where V_{wg} is the volume of the tube walls of the GHRC, ρ_{wg} is the density of the metal in the wall or the fins of the GHRC, C_{wg} is the specific heat of the wall or fin of the GHRC, and n_{tg} is the number of tubes in the GHRC.

Fins:

$$V_{fg}\rho_{wg}C_{wg}n_{fg}n_{tg} = (0.346\times10^{-5})(500)(0.11)(641)(56) = 68.3 \text{ Btu/}^{o}\text{F}$$

where V_{fg} is the volume of the fins of the GHRC and n_{fg} is the number of fins per tubes in the GHRC.

NaK Inventory:

$$M_{ng}C_{n} = (12.6)(0.21) = 2.6 \text{ Btu/}^{o}\text{F}$$

where M_{ng} is the mass of NaK in GHRC, and C_{n} is the specific heat of NaK.

APPENDIX B

DERIVATION OF ERROR FUNCTION OF AIRFLOW INTEGRAL FEEDBACK CONTROL

The linearized feedback integral control loop for the heat-exchanger system is shown in figure 19. The error function E_t for a disturbance in T_{ni} is given by equation (B1)

$$E_t(s) = \frac{\left(\frac{\partial f}{\partial T_i} F_t - \frac{\partial g}{\partial T_i} G_t\right)\Delta T_i}{1 + \frac{K_c G_a}{s}} \tag{B1}$$

where

$$K_c = \frac{1}{\tau_i} \frac{\partial w_a}{\partial e} \frac{\partial g}{\partial w_a}$$

Similarly, the error E_w for a NaK flow disturbance is given by

$$E_w(s) = \frac{\left(\frac{\partial f}{\partial w_n} F_w - \frac{\partial g}{\partial w_n} G_w\right)\Delta w_n}{1 + \frac{K_c G_a}{s}} \tag{B2}$$

The numerators of equations (B1) and (B2) represent the input error signals to the feedback controller. This error is attenuated by the term in the denominator that represents the feedback controller. It is the attenuation as a function of frequency which determines the performance of the feedback controller.

The frequency response characteristic of the feedback loop error is determined by the structure of the G_a transfer function and the gain of the controller K_c. Assuming that G_a is of the form given in equation (6), the transfer function of the feedback controller loop error G_f takes the form

$$G_f(s) = \frac{\frac{s}{K_c}\left(1 + \frac{\tau_a s}{2}\right)^2}{1 + \frac{s}{K_c} + \frac{\tau_a s^2}{K_c} + \frac{\tau_a^2 s^3}{K_c}} \tag{B3}$$

The gain is adjusted for critical damping, which is obtained when the third-order polynomial in the denominator factors into the form $(1 + \tau_1 s)(1 + \tau_2 s)^2$. To solve for K_c the preceding expression is set equal to the denominator:

$$1 + (\tau_1 + 2\tau_2)\, s + \left(2\tau_2\tau_1 + \tau_2^2\right)s^2 + \tau_1\tau_2^2 s^3 = 1 + \frac{s}{K_c} + \frac{\tau_a s^2}{K_c} + \frac{\tau_a^2 s^3}{4K_c}$$

Equating the coefficients of each power of s results in three simultaneous equations for the three unknowns τ_1, τ_2, and K_c:

$$\frac{1}{K_c} = \tau_1 + 2\tau_2$$

$$\frac{\tau_a}{K_c} = 2\tau_2\tau_1 + \tau_2^2$$

$$\frac{\tau_a^2}{4K_c} = \tau_1\tau_2^2$$

Solving these equations yields the following values for the unknowns:

$$\tau_1 = \frac{3}{8}\tau_a$$

$$\tau_2 = \frac{3}{2}\tau_a$$

$$\frac{1}{K_c} = \frac{27}{8}\tau_a$$

Substituting these values into equation (B3) results in the following equation:

$$G_f(s) = \frac{3.375\ \tau_a s(1 + 0.5\ \tau_a s)^2}{(1 + 0.375\ \tau_a s)(1 + 1.5\ \tau_a s)^2} \tag{B4}$$

when the frequency of the disturbances in normalized form is defined so that $jw = 0.5\ \tau_a s$, equation (B4) takes on the more general form given in equation (B5)

$$G_f(j\omega) = \frac{6.57\ j\omega(1 + j\omega)^2}{(1 + 0.75\ j\omega)(1 + 3j\omega)^2} \tag{B5}$$

REFERENCES

1. Anon.: Proceedings of the AIAA First Rankine Cycle Space Power System Specialist Conference, October 26-28, 1965. AEC Rep. No. CONF-651026, Vol. 1, 1965.

2. Stout, Thomas M.: A Note on Control Area. J. Appl. Phys., vol. 21, no. 11, Nov. 1950, pp. 1129-1131.

3. Smith, Richard L.; Mealey, Charles W., Jr.; Kadow, Charles F.; Brenza, Arthur D.; Bell, Richard N.; Sturman, John C.; and Perry, Allen L.: A Central Facility for Recording and Processing Transient-Type Data. NASA TN D-1320, 1963.

TABLE I. - COMPARISON OF HEAT CAPACITIES AND NaK DWELL TIMES OF SPACE RADIATOR AND TEST-FACILITY HEAT EXCHANGER

Property	Radiator	Heat exchanger
NaK inventory, lb	53.8	12.7
Heat capacity of NaK in tubes, Btu/^{o}F	11.3	2.6
Heat capacity of tubes, Btu/^{o}F	278.5	28.9
Heat capacity of fins, Btu/^{o}F	83.2	68.3
Total heat capacity, Btu/^{o}F	373.	100.
Dwell time, NaK at rated flow (11.1 lb/sec), sec	4.9	1.1

TABLE II. - TIME CONSTANTS USED FOR RADIATOR SIMULATION[a]

Time constant	Time-constant value, sec	Method of determination
τ_a	67	Experimental
τ_{wg}	48	Experimental
τ_{tg}	75	$\frac{C_g}{2w_nC_n}\left(1+\frac{\partial g}{\partial T_i}\right)$
τ_{wf}	120	$\frac{C_f}{2w_nC_n}$
τ_{tf}	190	$\frac{C_f}{2w_nC_n}\left(1+\frac{\partial f}{\partial T_i}\right)$

[a]Values of w_n = 27 000 lb/hr, and $\partial f/\partial T_i \cong \partial g/\partial T_i \cong 0.6$ were used for the calculations.

TABLE III. - POTENTIOMETER SETTINGS FOR ANALOG

COMPUTER PROGRAM OF RADIATOR

SIMULATOR CONTROLLER

Potentiometer number	Potentiometer setting	Equation and explanation
2	0.6304	Adjusted for correct scaling
3	.1001	$10/\tau_d$
4	.1000	
5	.1000	
6	.1000	
7	.4067	Scaling factor
11	.5000	Constant set to 0.50
12	.5000	Constant set to 0.50
13	1.0000	$K_t = 1.0$
14	------	Gain (variable)
15	1.0000	$K_t = 1.0$
16	------	Gain (variable)
20	.0038	$(3/\tau_{tf})\left[1 + 2.25\left(\tau_a/\tau_{tf}\right)^2 - (3\tau_a/\tau_{tf})\right]$
21	0	Bias
22	.0078	$9\tau_a/\tau_{tf}^2\left[1 - (3/2)(\tau_a/\tau_{tf})\right]$
24	.0160	$3/\tau_{tf}$
26	.0158	$3/\tau_{tf}$
27	.0044	$6.75\left(\tau_a^2/\tau_{tf}^3\right)$
28	.0159	$3/\tau_{tf}$
32	.622	0.622 (scale factor)
33	0	Input signal bias
34	.0094	$1.125/\tau_{wf}$
35	.2937	$0.2[(\tau_a/\tau_{wg}) - 0.66]$
36	.0167	$2/\tau_{wf}$
37	.0074	$0.75/\tau_{wf}$
38	.0156	$2/\tau_{wf}$
39	.0083	$\left[(\tau_a/\tau_{wg}) - 1\right]/\tau_{wg}$
40	.0209	$(\tau_{wg})^{-1}$
62	.1455	Valve bias (variable)
64	.2095	Valve bias (variable)
65	.4089	Scale factor 0.4067
66	.5912	Scale factor
68	------	Integration time (variable)

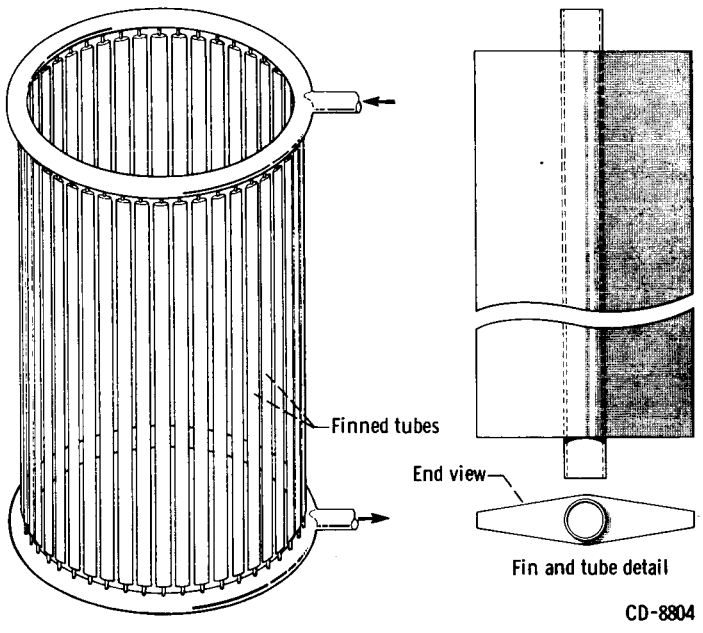

Figure 1. - Cylindrical radiator (FHRC) used as model (130 parallel finned tubes).

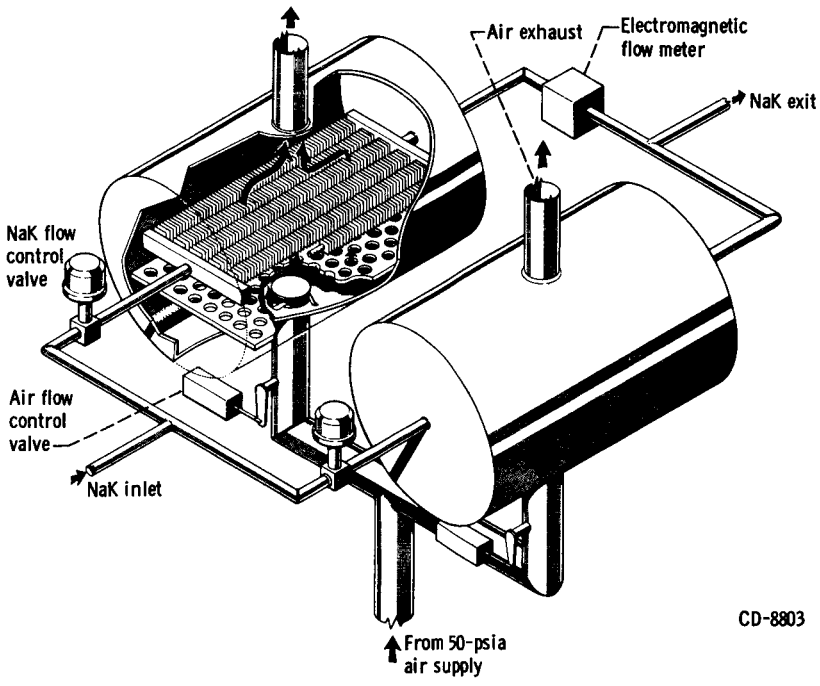

(a) Overall facility.

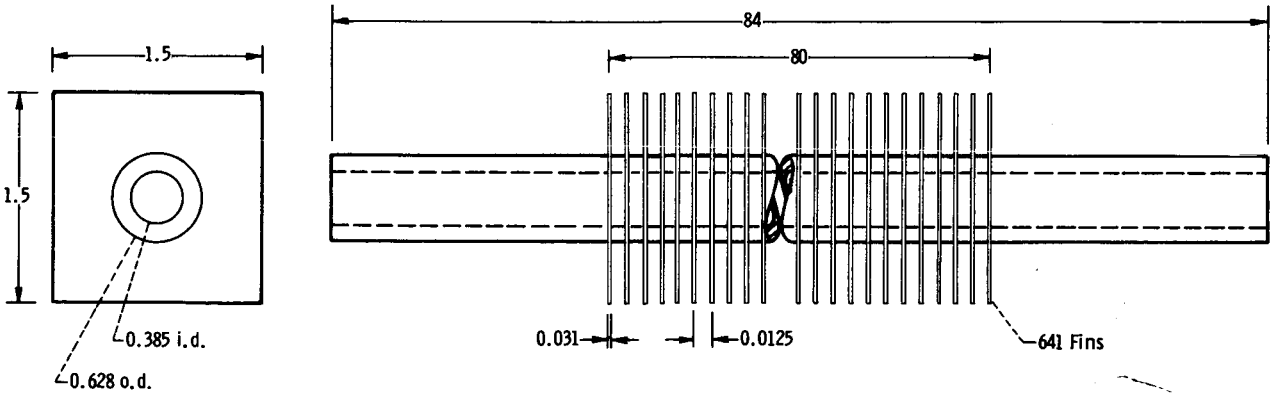

(b) Finned-tube detail. (All dimensions are in inches.)

Figure 2. - Test-facility air-blast heat exchanger (GHRC) used in simulation of space radiator.

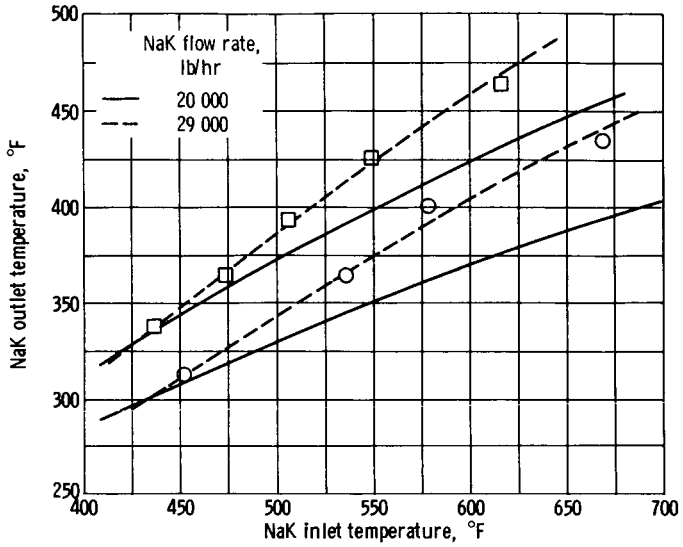

Figure 3. - Comparison of uncontrolled heat-exchanger characteristics with those of assumed flight radiator model for steady-state conditions. Heat exchanger properties: 56 finned tubes; constant coolant airflow. Radiator properties: cylindrical; 130 finned tubes; sun operation; emissivity, 0.90; absorptivity, 0.40.

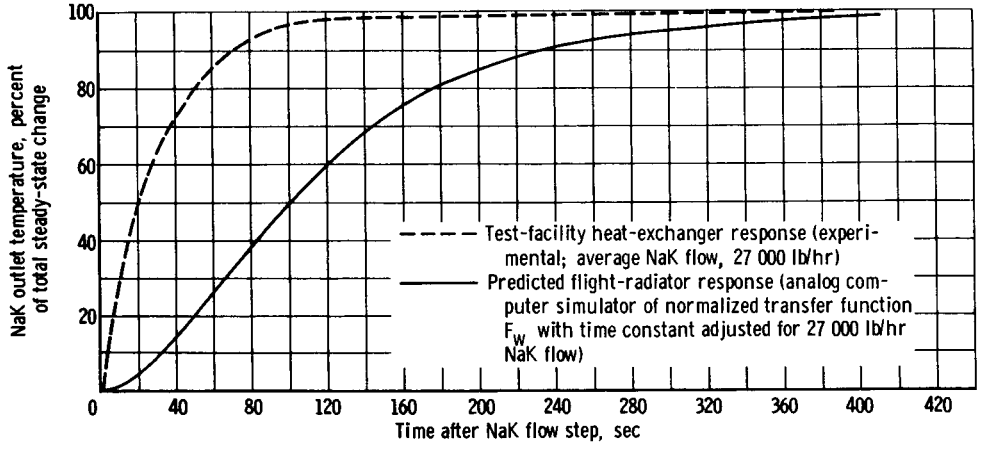

Figure 4. - Comparison of NaK outlet-temperature responses for uncontrolled GHRC and assumed FHRC subjected to identical NaK flow steps.

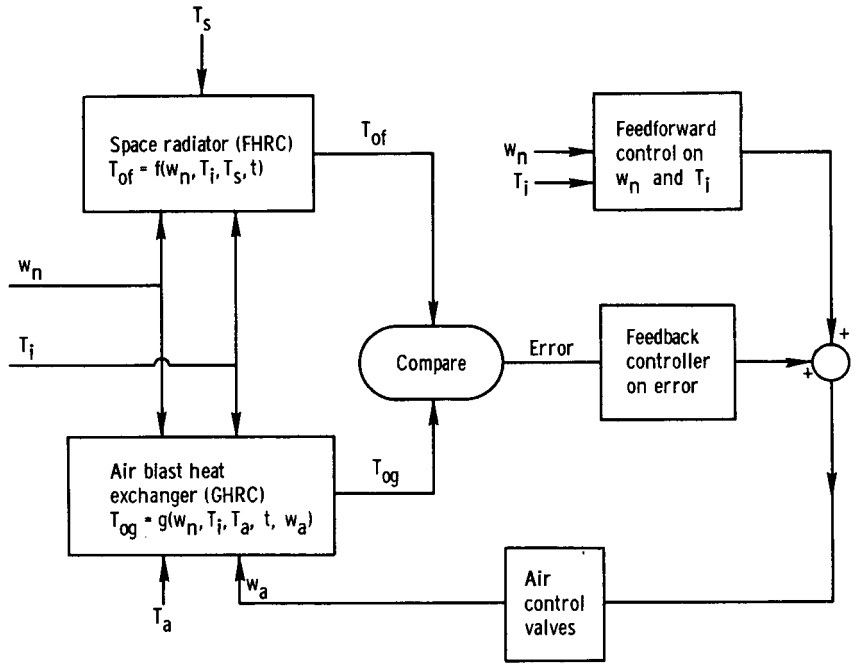

Figure 5. - Control system concept for simulating space radiator incorporating both feedback and feedforward control.

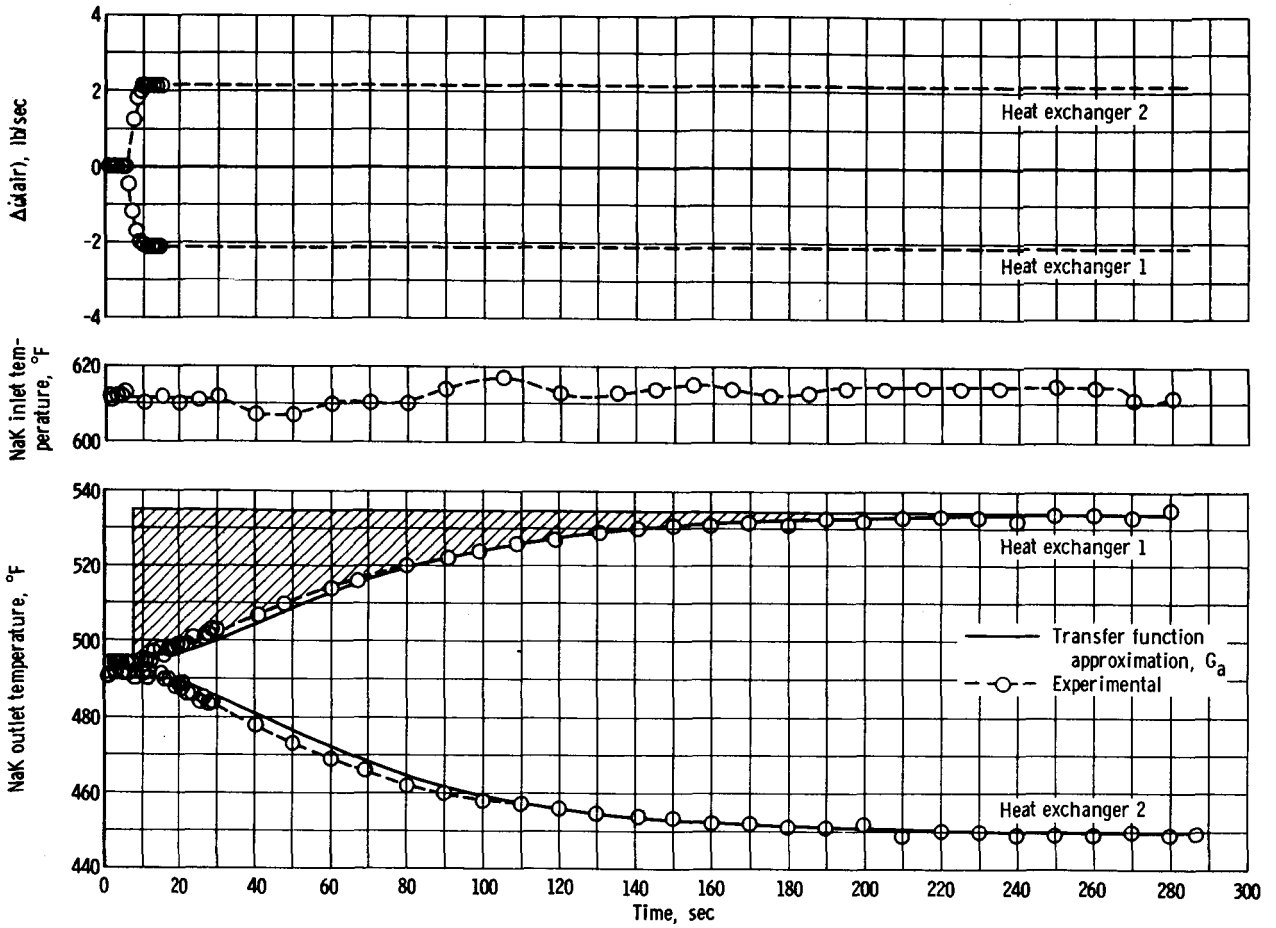

Figure 6. - Heat-exchanger transient response to step change in coolant air-flow showing method of control-area calculation and comparison with transfer function approximation ($G_a = 1/[1 + (\tau_a s/2)]^2$).

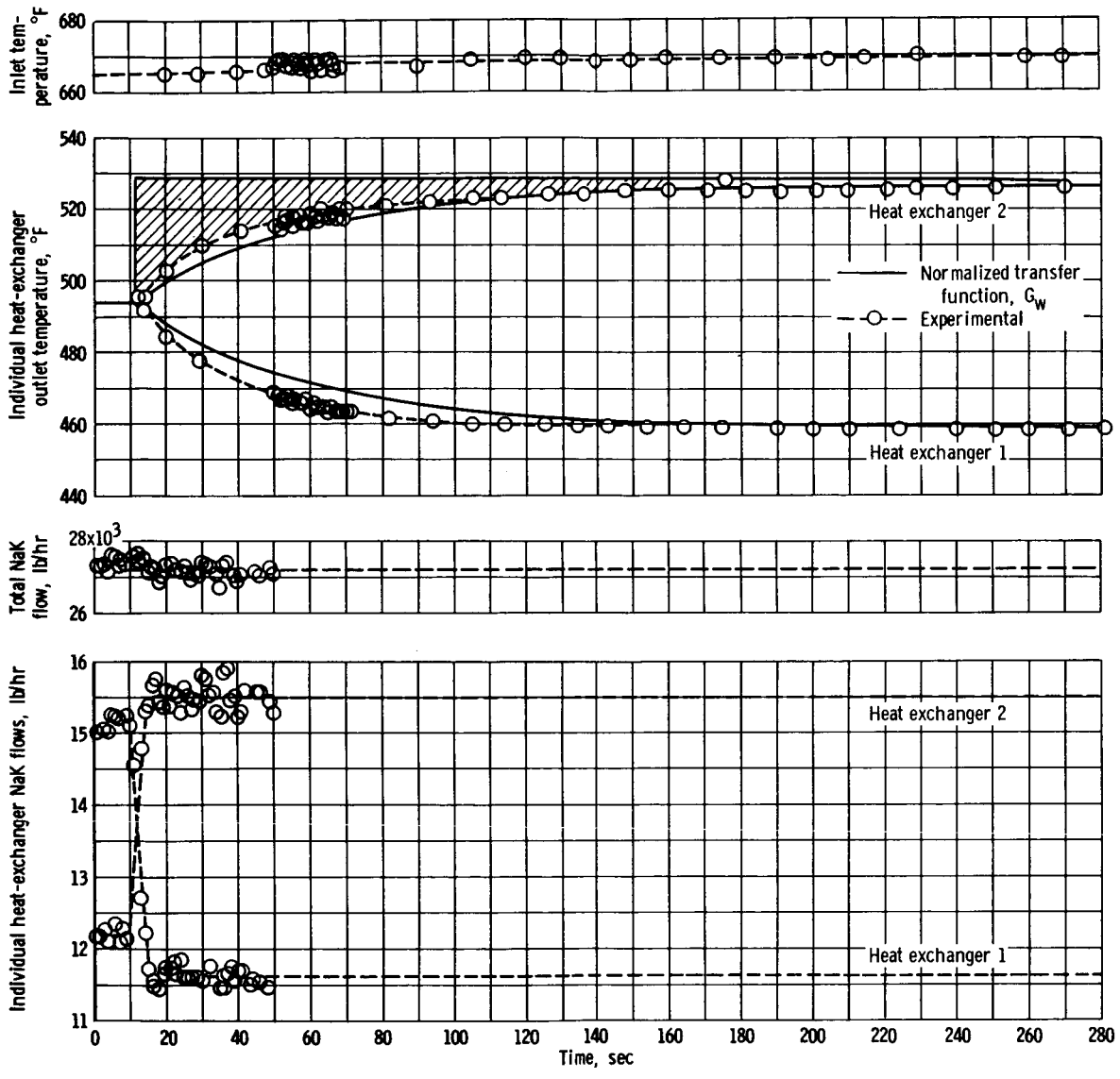

Figure 7. - Heat-exchanger transient response to step change in NaK flow used for estimating normalized transfer function ($G_w = 1/(1 + \tau_{wg}s)^1$).

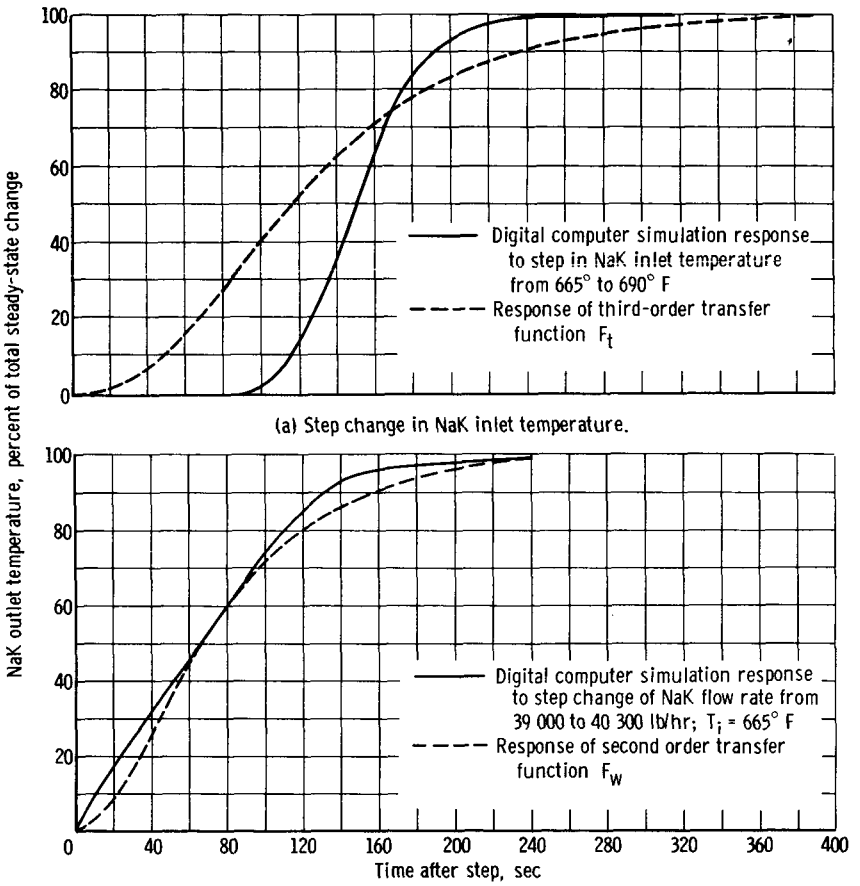

Figure 8. - NaK outlet temperature responses to NaK input variables comparing transfer function approximations to digital computer simulation of flight radiator. Time constant adjusted for NaK flow of 39 000 pounds per hour.

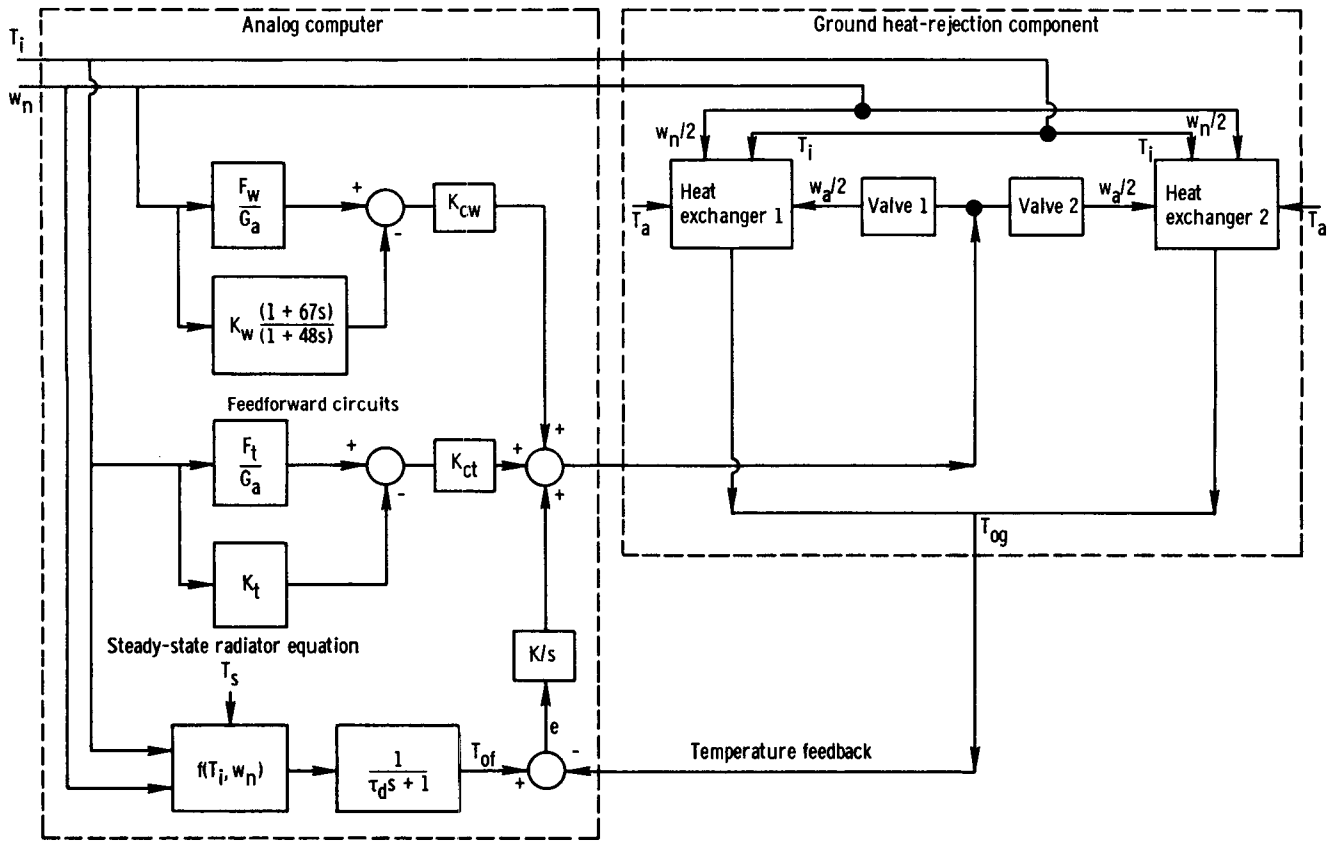

Figure 9. - Block diagram of complete radiator simulator showing feedforward and feedback control elements as well as ground heat-rejection component.

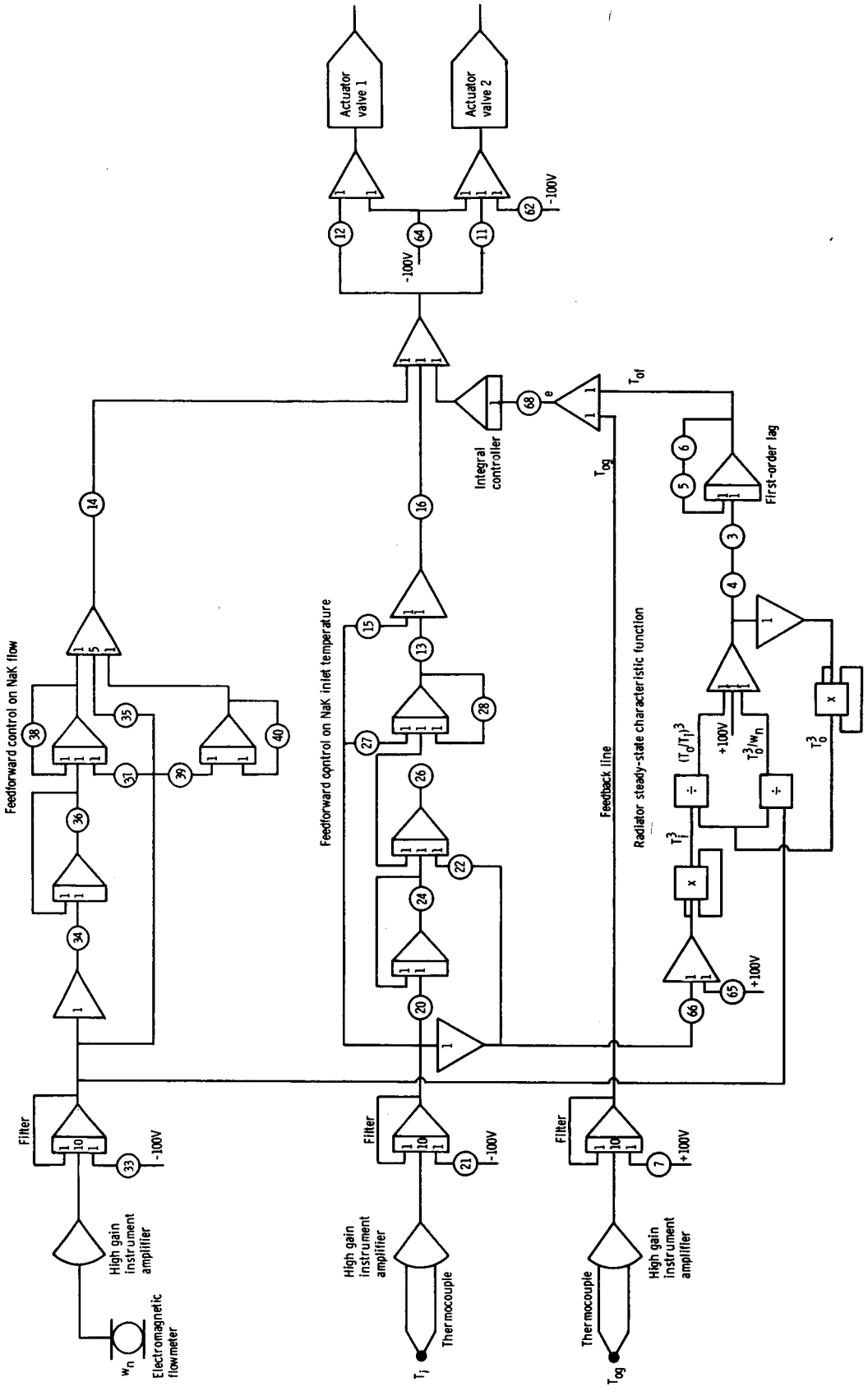

Figure 10. - Analog computer program for radiator simulator.

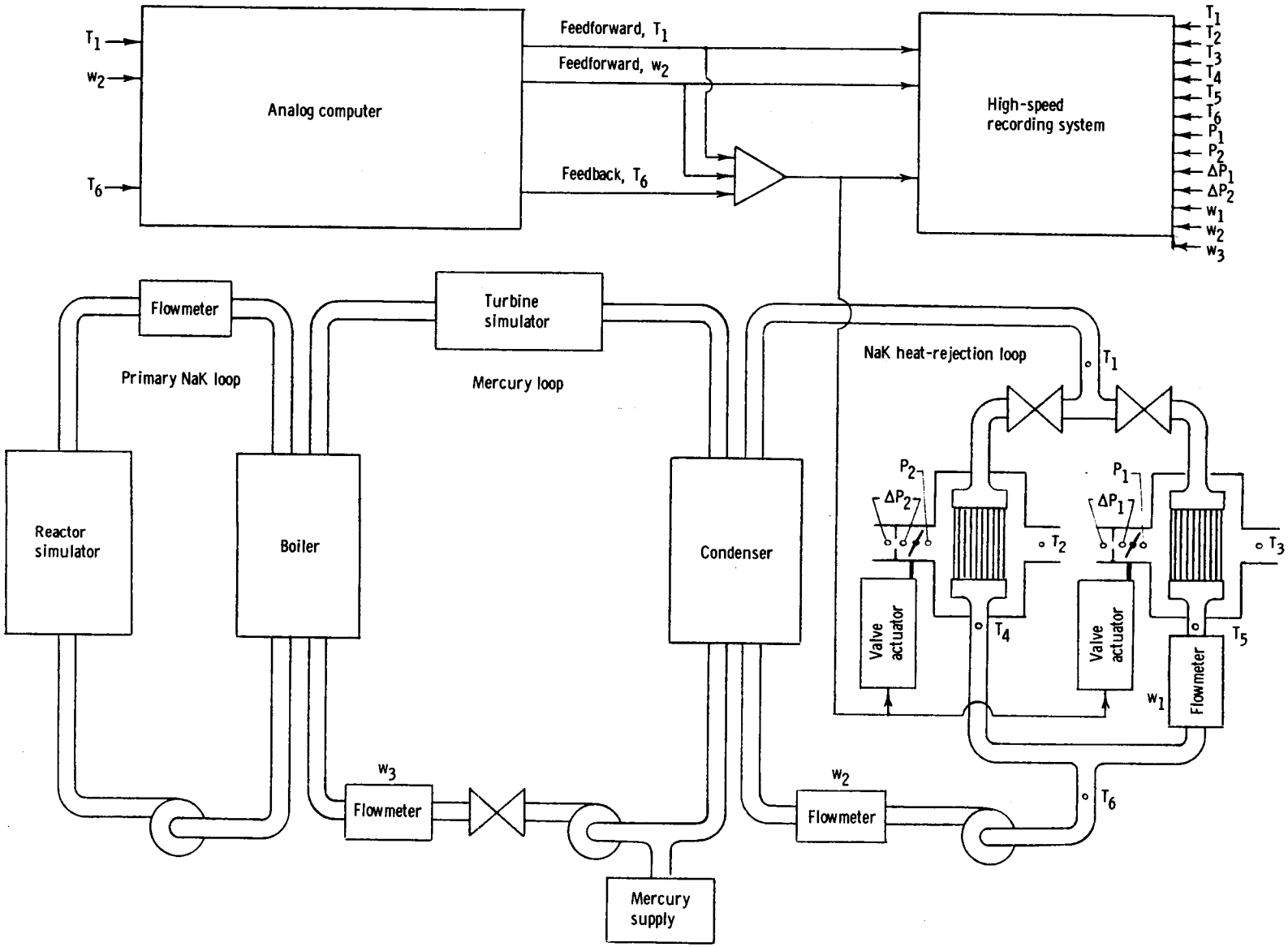

Figure 11. - SNAP-8 simulator facility showing primary instrumentation used for radiator simulator testing. (Symbols indicate location and type of instrumentation: w = flow; T = temperature; P = pressure.)

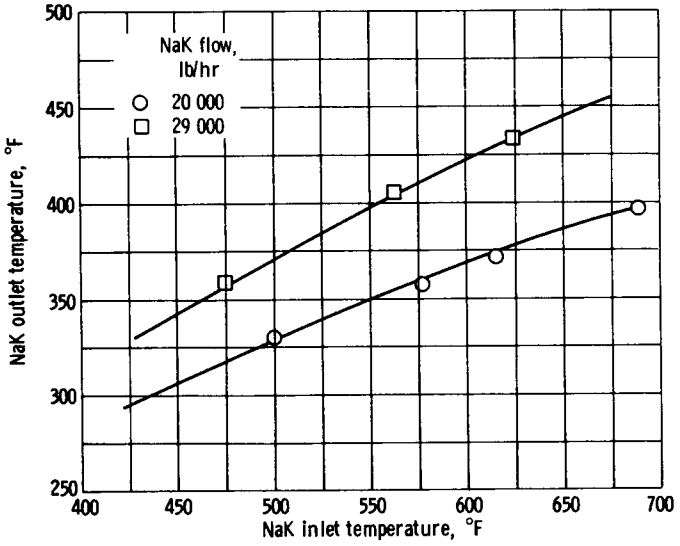

Figure 12. - Radiator simulator steady-state data compared with predicted space radiator characteristics. 130-Tube cylindrical radiator properties: sun operation; emissivity, 0.90; absorptivity, 0.40.

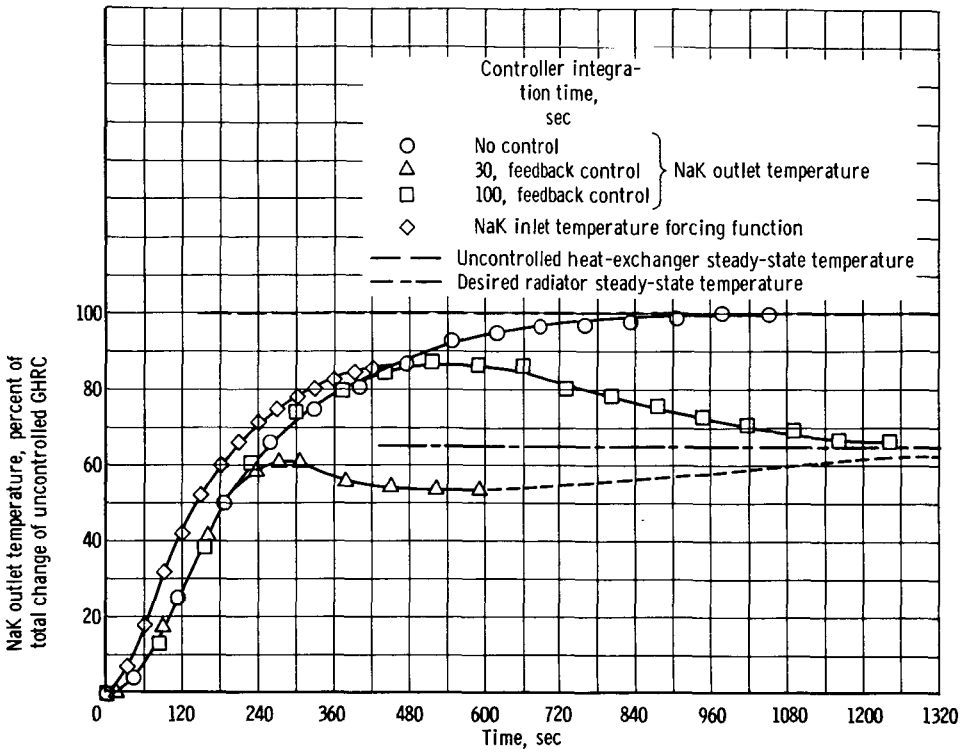

Figure 13. - Transient response of GHRC outlet temperature due to inlet temperature disturbances for various values of integral feedback control times. Temperature disturbance was introduced by ±12-percent steps in mercury flow: Typical initial conditions: inlet temperature, 550° F; outlet temperature, 400° F; NaK flow, 29 000 pounds per hour; power level, 325 kilowatts.

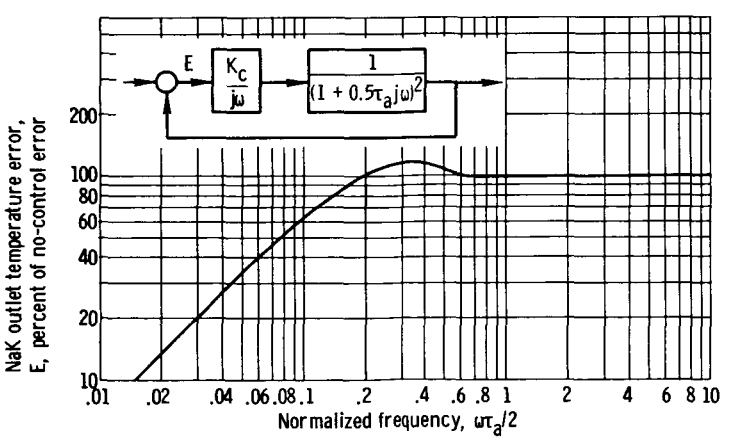

Figure 14. - Amplitude of NaK outlet temperature error as function of frequency of input disturbance to integral feedback controller.

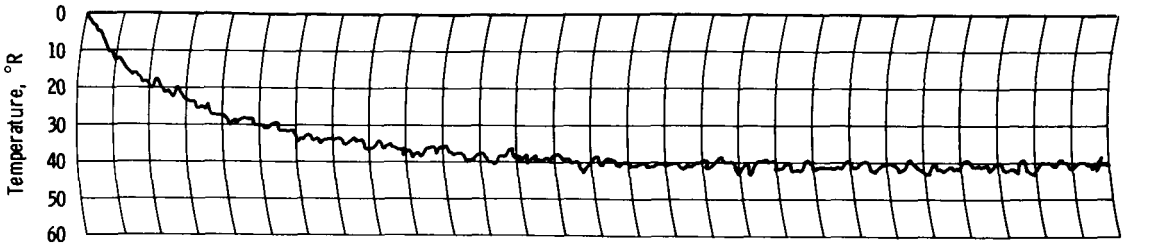

(a) NaK inlet-temperature transient. Power stepped from 325 to 380 kilowatts.

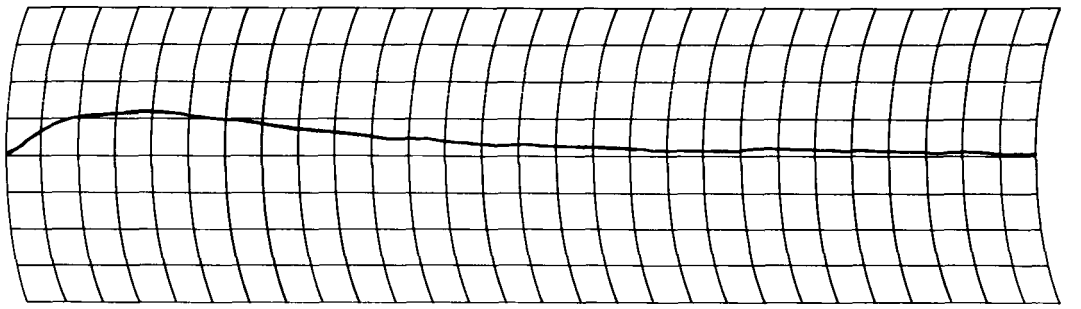

(b) Feedforward signal from NaK inlet-temperature compensating circuit.

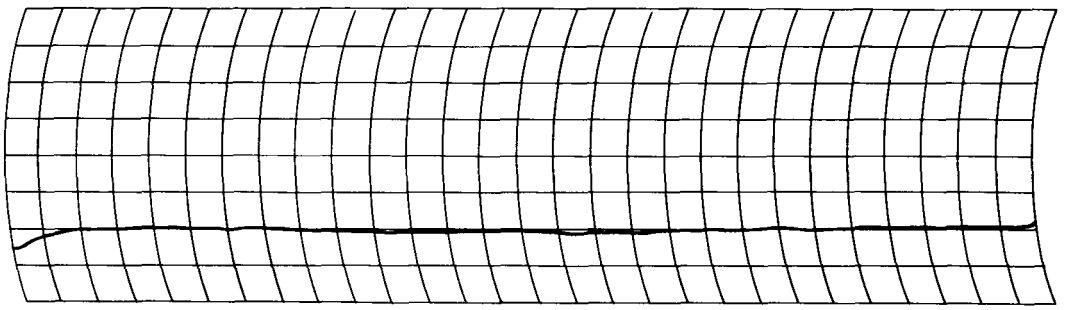

(c) Combined feedforward and feedback signal to control valves.

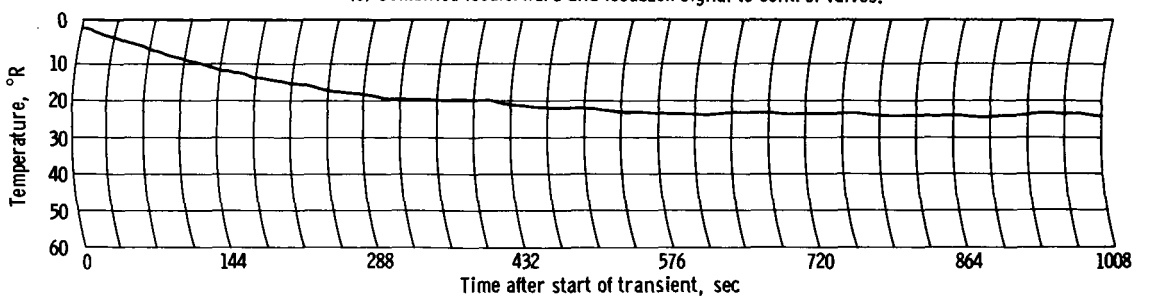

(d) NaK outlet-temperature transient.

Figure 15. - Example of radiator simulator transient response to step change in mercury flow.

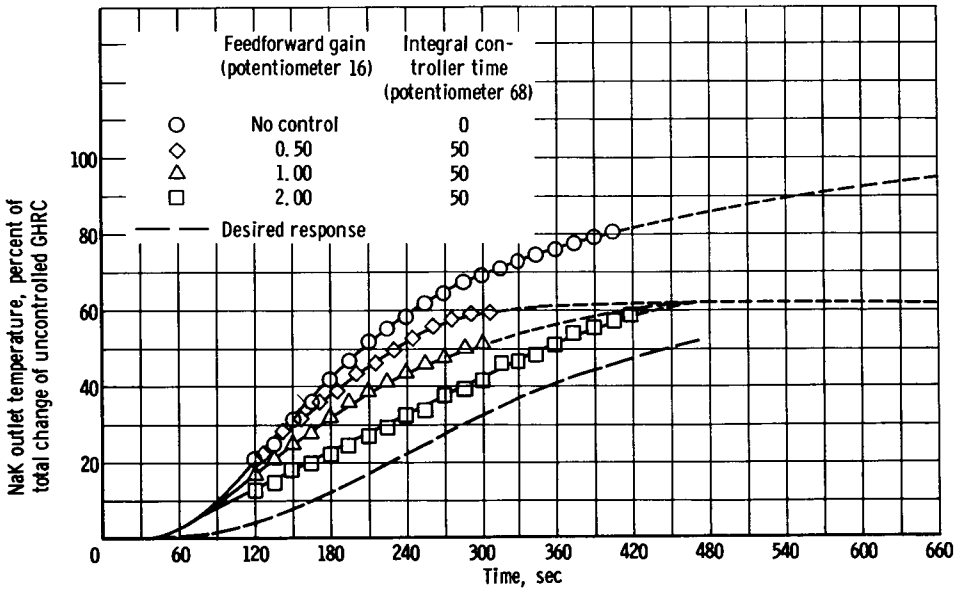

Figure 16. - NaK outlet-temperature response to NaK inlet-temperature transient showing effect of feedforward circuit gain. Disturbance introduced by 12-percent step in mercury liquid flow; operating power, approximately 340 kilowatts; NaK flow rate, 29 000 pounds per hour; inlet temperature, 550° F; outlet temperature, 400° F.

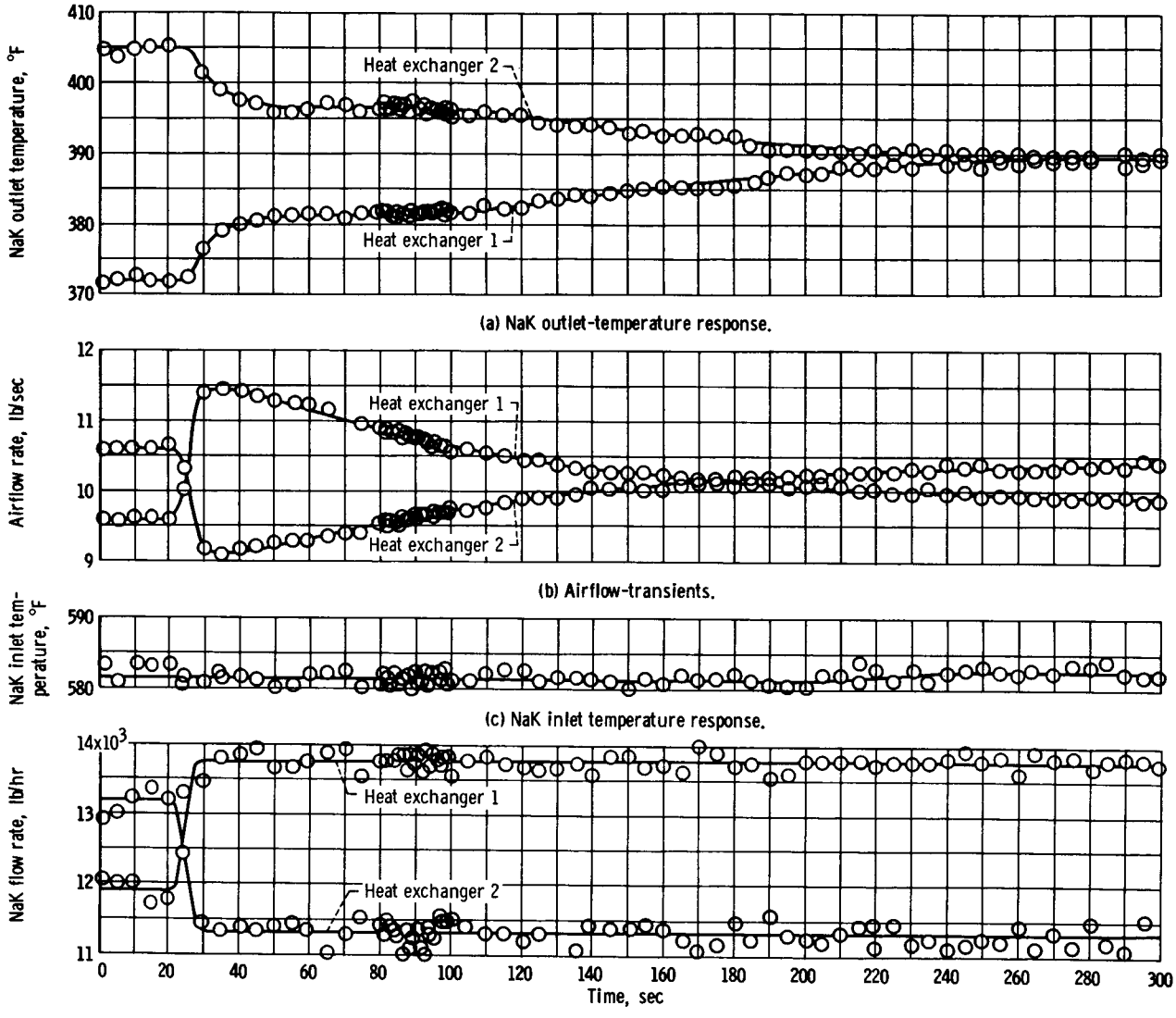

Figure 17. - Typical response of radiator simulator to step changes in NaK flow rate.

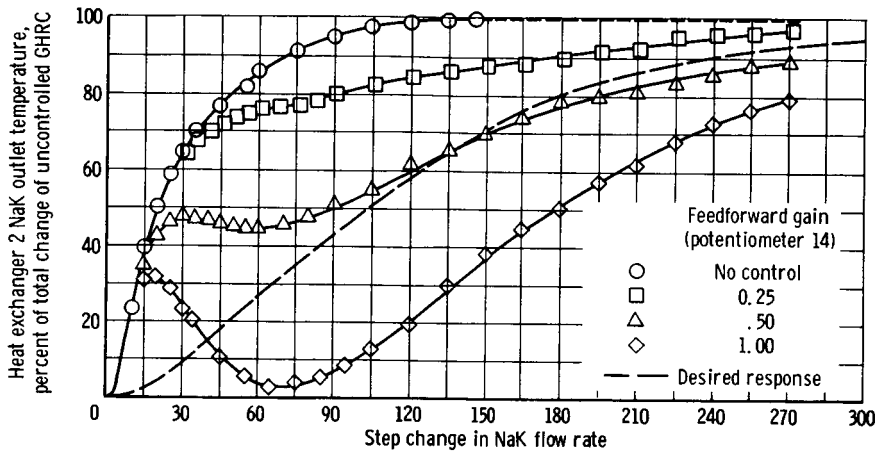

Figure 18. - NaK outlet-temperature-transient response to ±10 percent step changes in NaK flow rate illustrating change due to variation in gain of NaK flow feedforward circuit. Feedback loop disconnected; typical operating level: NaK flow rate, 25 000 pounds per hour; NaK inlet temperature, 580° F; power, 350 kilowatts.

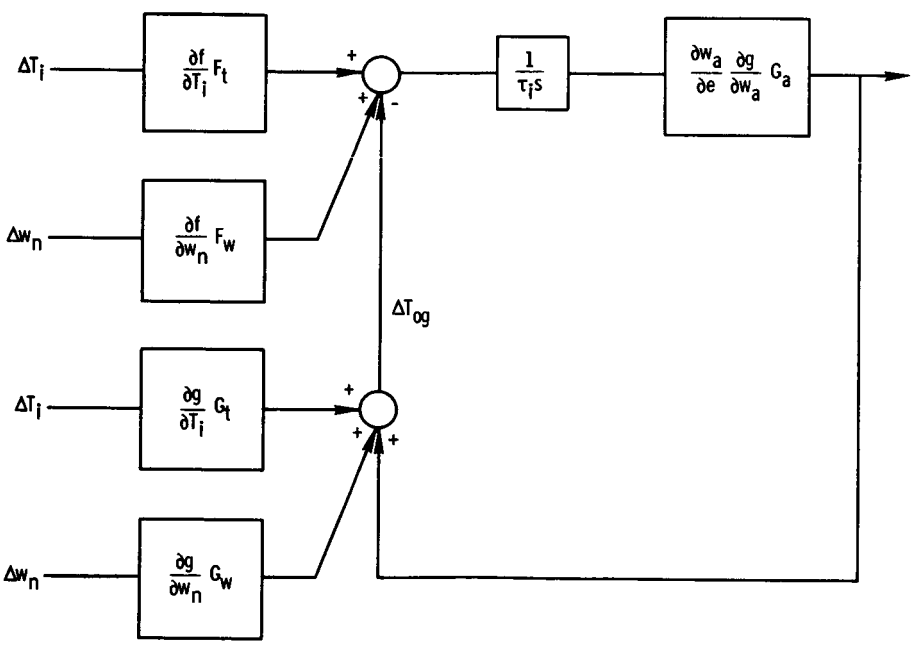

Figure 19. - Simplified block diagram of radiator feedback control system.